



Budapesti Műszaki és Gazdaságtudományi Egyetem

Szélessávú Hírközlés és Villamosságtan Tanszék



Department of Broadband Infocommunication and Electromagnetic Theory,
Faculty of Electrical Engineering and Informatics,
Budapest University of Technology and Economics

Evaluation of Electromagnetic Metamaterials

Monograph for the

Department of Broadband Infocommunication and Electromagnetic Theory

Authors:

Zsolt Szabó (PhD) Associate Professor

Arnold Kalvach PhD student

Zoltán Szalay PhD student

Budapest, 2013

1. Introduction

One could think that with the formulation of Maxwell equations all electromagnetic phenomena are very well understood. According to our observations, magnetism vanishes for all natural materials at higher frequencies, and the refractive index is always positive. However, novel types of artificial composite materials called metamaterials were demonstrated which have the striking property of negative refractive index. The concept of metamaterial was coined by Veselago, who investigated theoretically how an electromagnetic wave would propagate in a material with negative refractive index [1]. The first physical realization of such a metamaterial was first presented by Smith in 2000 for microwave frequencies [2]. Since then the research of metamaterials exponentially increased over the last years. With metamaterials the researchers are expecting to produce revolutionary new devices like multi-wavelength compact antennas for telecommunication or superlenses to push the limits of optical imaging and lithography [3], [4].

The response of a material to electromagnetic waves is dictated by its complex refractive index $N = n + i\kappa$, where n is the real part of the refractive index and κ is the extinction coefficient. From Maxwell's equations it follows that the refractive index N can be expressed as a function of the complex electric permittivity and magnetic permeability $N = \sqrt{\mu_r \varepsilon_r}$. The square root of a function can have a positive or negative value. As it was presented in [1], [4], the Maxwell equations imply the selection of the negative sign of the refractive index when the real parts of the electric permittivity and of the magnetic permeability are both negative. In addition, to satisfy the causality principle, the permittivity and permeability must be dispersive.

All known natural materials have positive refractive index. What can be the reason behind the fact that there are no natural negative refractive index materials? In undergraduate classes on Electromagnetics [5] it is observed that Maxwell's equations are not symmetrical in the presence of charges and current densities. The symmetry of the equations can be recovered by introducing magnetic charge and currents, however they were never observed in any experiment. It is interesting to note that the existence of the magnetic charge would explain the quantization of the electric charge as it was shown by Dirac in 1931 [6]. The electric field has stationary sources, but the magnetic field is always divergence free and it is caused by moving electric charges. The magnetic response at high frequencies vanishes because the magnetic spin cannot follow the optical frequencies. In addition, by comparing the radiated power of oscillating electric and magnetic dipoles, it can be observed that the electric dipole radiation always dominates. Special arrangements are needed to expose the magnetic dipole radiation at a macroscopic scale. At the end the absence of the magnetic charge implies that there are no natural materials with negative refractive index.

A material with negative refractive index can be produced by the superposition of manufactured structures with negative permittivity and negative permeability. The metals contain a large number of free electrons, and their electromagnetic behavior can be accurately represented by the Drude model. Below the natural plasma frequency the metals have negative dielectric constant. The motion of the electrons can be confined by micro- or nano-structuring, which moves the plasma frequency to smaller frequencies. A very common design of an artificial dielectric with tailored negative permittivity is the wire medium [7]. The design of materials with any magnetic response at frequencies ranging from microwaves to optical wavelengths by itself is not an easy task. The additional challenge is the design of a structure with sufficiently strong magnetic resonance to provide negative magnetic permeability. At gigahertz or terahertz frequencies the most common designs to produce artificial magnetism are the variations of the split ring resonator structure [8], [9], [10]. At optical wavelengths, due to the fabrication difficulties and the increased losses and reduced power handling capacity of the split ring structures of reduced size, new designs like pairs of nanorods [11] or fishnet structures [12], [13], [14] were proposed. The final goal of the metamaterial research is to design low-loss composite structures which can operate at frequencies from microwaves to optical wavelengths and to tailor the refractive index of these structures to any positive or negative value.

By reviewing the literature presenting metamaterial designs and simulations we can note that several of them use the CST Microwave Studio [14], [15], [16], [17], [18]. Internet forums often pose questions referring to metamaterial simulation and effective metamaterial parameter extraction. Therefore in this paper, we present a detailed guide on how to extract the effective metamaterial parameters and how to model metamaterial structures with CST Microwave Studio. The applicability and the limits of the presented method will be illustrated by extracting the effective metamaterial parameters of single and multilayer fishnet structures.

2. Effective metamaterial parameter extraction method

Several effective metamaterial parameter retrieval techniques exist in literature [19], [20], [21], [22], [23], [24], [25]. In this paper we introduce the complex effective electric permittivity and magnetic permittivity in such a way, that a homogeneous slab with these electromagnetic parameters gives the same electromagnetic response as the metamaterial slab.

The validity of this simplification must be carefully checked for each particular metamaterial. The effective medium theory cannot describe the electromagnetic behavior of metamaterials when higher order modes can propagate, or Bragg diffraction occurs due to periodicity. Unfortunately there is no clear guideline on how to decide when the effective medium theory approach is valid. The usual suggestion is that the effective medium theory can be applied to a system composed of elements which are much smaller in size than the wavelengths of operation. However, it is well known, that in a dielectric slab where the magnitude of the refractive index is larger than one, the wavelength is smaller than the free-space wavelength $\lambda_{opt} = \lambda / n$, where λ_{opt} is the optical wavelength (the wavelength in the dielectric) (Zsolt, I suggest that the term “optical wavelength” restricts your definition to the visible spectrum, while your considerations apply to all frequency ranges. People often use the term “guided wavelength” or “wavelength in the medium” instead), and λ is the free space wavelength. To decide whether a dielectric slab is optically thick or thin, the optical wavelength should be compared to the thickness of the sample (For the dielectric to be optically thick or thin is a separate issue from being considered a material, and does not necessarily provide a criterion for the applicability of the effective medium theory. In case of metamaterials the effective material parameters are not known a priori, therefore we cannot determine in advance the validity of the effective medium theory (If a metamaterial is not a material then the effective medium theory is not applicable). As it is presented in the following, the mathematical solution of the effective metamaterial extraction procedure is generally not unique. When the algorithm cannot find any physically justified solution, the limits of the effective medium theory are reached.

The electromagnetic behavior of most metamaterial designs is anisotropic, requiring a tensor to properly describe it. Furthermore, a negative refractive index is only possible when the metamaterial is excited by a plane wave with a specific polarization direction and angle of incidence (This is not generally true since one can build metamaterials that, like Cartesian meshes for numerical field solver algorithms, have negative refractive index in arbitrary direction, thus making them suitable for applications that involve fields other than plane waves). Even when all elements of the full permeability and permittivity tensor are determined, the model can predict just the far field behavior, while the near field behavior of the metamaterial is lost. For most metamaterial devices, the coupling effects between the metamaterial and the surrounding structures cannot be neglected. Hence a full-wave simulation must be performed to obtain the correct electromagnetic behavior. (I would even say that applications of metamaterials using only the far field are of little practical interest since the only function they have is to produce a given phase shift of the transmitted and reflected plane wave).

In spite of these limitations, the effective material parameters can be useful in designing optimal metamaterial unit cells with a computer. For example, the bandwidth of negative refractive index can be maximized and/or the losses can be reduced. Due to the high computational cost of the electromagnetic field solution, the metamaterial geometry in a first design phase can be optimized for a specific polarization and angle of incidence. For this purpose a robust and fast effective metamaterial parameter retrieval procedure is required.

Our effective metamaterial retrieval procedure [25] is summarized in the following. Applying the Fresnel-Airy formulas for a homogeneous slab, the wave impedance can be uniquely determined. However, the calculation of the refractive index involves the evaluation of a complex logarithm. The complex logarithmic function is a multi-valued function [26]. The resulting uncertainty is referred to as branching problem, which affects only the real part of the refractive index. To remove this ambiguity, the Kramers-Kronig relation can be applied to estimate the real part of the refractive index from the imaginary part. The physically realistic exact values of the refractive index are determined by selecting those branches of the logarithmic function which are closest to those predicted by the Kramers-Kronig relation. The algorithm also enforces the continuity of the refractive index versus frequency.

For a plane wave with normal incidence on a homogeneous slab, the Fresnel-Airy formulae relate the wave impedance and the refractive index to S-parameters as

$$S_{11} = \frac{R_{01}(1 - e^{i2N_{eff}k_0d_{eff}})}{1 - R_{01}^2e^{i2N_{eff}k_0d_{eff}}}, S_{21} = \frac{(1 - R_{01}^2)e^{iN_{eff}k_0d_{eff}}}{1 - R_{01}^2e^{i2N_{eff}k_0d_{eff}}}, R_{01} = \frac{Z_{eff} - 1}{Z_{eff} + 1}, \quad (1)$$

where $N_{eff}(\omega) = n_{eff}(\omega) + i\kappa_{eff}(\omega)$ is the complex effective refractive index, Z_{eff} is the complex effective wave impedance, k_0 is the free space wave number, d_{eff} is the effective thickness of the metamaterial slab (how do you define effective thickness with respect to geometrical thickness?), and ω is the angular frequency. From the previous relations we find:

$$Z_{eff} = \pm \sqrt{\frac{(1 + S_{11})^2 - S_{21}^2}{(1 - S_{11})^2 - S_{21}^2}}, \quad (2)$$

$$e^{iN_{eff}k_0d_{eff}} = \frac{S_{21}}{1 - S_{11}R_{01}}. \quad (3)$$

When the magnitude of Z_{eff} is large enough (what is enough?), then the condition $\text{Re}(Z_{eff}) > 0$ is applied to determine the sign of (2). When the magnitude is small, numerical or measurement errors can lead to an incorrect sign in (2), therefore the condition $|e^{iN_{eff}k_0d_{eff}}| \leq 1$ is applied to determine the sign of the wave impedance [19], [25]. The complex refractive index can be calculated as

$$N_{eff} = \frac{1}{k_0d_{eff}} \left\{ \text{Im} \left[\ln \left(e^{iN_{eff}k_0d_{eff}} \right) \right] + 2m\pi - i \text{Re} \left[\ln \left(e^{iN_{eff}k_0d_{eff}} \right) \right] \right\} = N_{eff}^0 + \frac{2m\pi}{k_0d_{eff}}, \quad (4)$$

where m is an integer denoting the branch index, and N_{eff}^0 is the complex refractive index corresponding to the principal branch of the logarithmic function. The parameter extraction procedure takes advantage of the fact that the imaginary part of the refractive index is not affected by the branches of the logarithmic function. Therefore it can be calculated from (4) without ambiguity. Knowing the imaginary part of the refractive index, we can determine the real part by applying the Kramers-Kronig relation

$$n^{KK}(\omega') = 1 + \frac{2}{\pi} P \int_0^{\infty} \frac{\omega \kappa_{eff}(\omega)}{\omega^2 - \omega'^2} d\omega \quad (5)$$

where P denotes the principal value of the improper integral. The limits of the integral are 0 and ∞ , therefore the values of the S-parameters must be known for the entire frequency range. Since this is not possible, the integral must be truncated, and the Kramers-Kronig relations yield an approximation of the refractive index. For accuracy, the range of the integration should be as large as possible. Since time domain methods yield the S-parameters over a large frequency range in a single run, they are particularly well suited to this algorithm. On the other hand, if the frequency becomes too large, we may reach a point where the concept of effective parameters is no longer meaningful, since the guided wavelengths are in the order of the characteristic dimensions of the metamaterial structure.

The branch number m is determined as

$$m = \text{Round} \left[\left(n^{KK} - n_{eff}^0 \right) \frac{k_0d_{eff}}{2\pi} \right]. \quad (8)$$

Therefore, the real part of the complex refractive index is calculated such that it is closest to the value predicted by the Kramers-Kronig relation. The branch number m is substituted in (4), and the exact value of the refractive index is calculated. Then the algorithm checks the continuity of the refractive index n . A discontinuity close to the limit of the calculation zone may be caused by the truncation error in the Kramers-Kronig integral. If the discontinuity is far from the limits of the covered frequency range and the discontinuity perseveres even when the frequency interval of the simulation is increased, this indicates that the limit of the effective medium theory is reached. Finally, the effective magnetic permeability and electric permittivity are calculated by the relations

$$\epsilon_{eff} = N_{eff} / Z_{eff}, \quad \mu_{eff} = N_{eff} Z_{eff}. \quad (9)$$

3. Effective metamaterial parameter extraction for the fishnet structure

To demonstrate the effective metamaterial parameter retrieval method, the fishnet structure presented in [15] is investigated. As it can be seen in Fig. 1.a, the fishnet metamaterial is a metal-dielectric-metal layered structure with rectangular holes. The thickness of the metal layers is 45 nm, and they are manufactured from silver. The dielectric is a 30 nm thick MgF₂ layer. The lattice constant is $a = 600$ [nm], the size of the unit cell is $w_x = 316$ [nm] and $w_y = 100$ [nm]. This metamaterial is operating at telecommunication frequencies, for a plane wave incident perpendicular to the surface and polarized along the x -direction. The electric permittivity of silver is represented by the Drude model

$$\varepsilon_r(\omega) = \varepsilon_\infty - \frac{\omega_p^2}{\omega(\omega - i\gamma_c)} \quad (10)$$

where $\varepsilon_\infty = 1$ is the electric permittivity at high frequencies, $\omega_p = 1.37 \cdot 10^{16}$ [rad/s] is the Drude plasma frequency and $\gamma_c = 8.5 \cdot 10^{13}$ [rad/s] the collision frequency. The exact permittivity values of the nano-structured silver layer can be obtained by fitting measured transmission-reflection data, resulting in a slightly higher collision frequency value than that obtained in case of a bulk material. As it can be observed in Fig. 1.b, by comparing the calculated and measured [27] values of the electric permittivity, the Drude model gives a good approximation for wavelengths larger than the natural plasma frequency. In the simulations, the separator MgF₂ layer is considered lossless with electric permittivity equal to 1.9044.

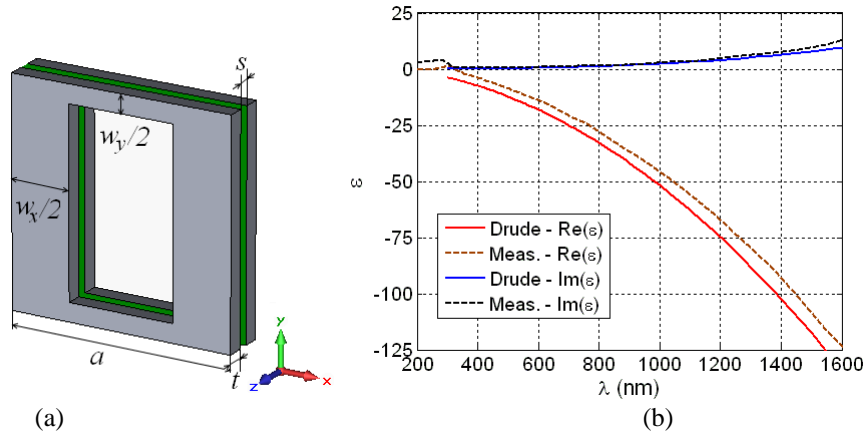


Fig. 1. The geometry of the fishnet unit cell (a) and the dispersive curve of silver (b). The solid line shows the Drude model approximation while the dashed lines are experimentally measured values.

As it was shown in [19], [20], for metamaterials with symmetrical geometry (in the direction of propagation of the electromagnetic wave), the effective thickness is just the sum of the lengths of unit cells it contains. The fishnet is symmetric with respect to the orientation and polarization of the incident wave, therefore no additional procedure is required to determine d_{eff} . The effective thickness in this case is $d_{eff} = 120$ nm.

One way to generate the S-parameters of a metamaterial slab is to model it with a three-dimensional electromagnetic field solver. In CST Microwave Studio the S-parameter calculation can be performed in many different ways. The very first choice is between the frequency domain solver and the time domain solver. In Fig. 2 three different ways are presented to calculate the S-parameters. Performing the calculations in more than one way gives the possibility to cross-check the results. The discretization of the structures can be different. For time domain solvers a rectangular mesh is preferred, while the frequency domain solver works with a tetrahedral mesh. In addition, all settings have advantages and restrictions. In CST Microwave Studio, the time domain calculations can simulate plane waves with perpendicular incidence. Oblique incidence can be simulated with a frequency domain solver and unit cell boundary conditions. However the unit cell boundaries cannot be in contact with anything else than air.

Meaningful material parameters can be defined for symmetric structures, where the extracted material parameters are independent of the direction of propagation. Therefore, the substrate is usually disregarded. In [15] the metamaterial is embedded in an effective dielectric medium with $\varepsilon_r = 1.21$ to

compensate for the red shift caused by the absence of the substrate. To allow the comparison between different solvers, the fishnet structure is suspended in air in the simulation presented in this paper.

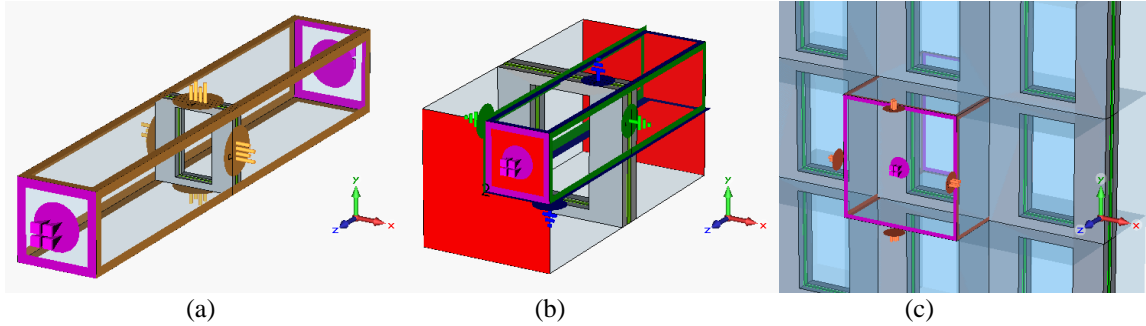


Fig. 2. Boundary conditions to calculate the S-parameters of the fishnet structure in three different ways, (a) refers to a time domain calculation with periodic boundary conditions and a plane wave source, (b) time domain calculation with PEC-PMC boundary conditions, (c) frequency domain calculation with unit cell boundary conditions and Floquet port excitation.

3.1 S-parameter calculation with a time domain solver specifying periodic boundary conditions and plane wave excitation

In this section, the S-parameters are calculated with the time domain solver by setting plane wave source and periodic boundary conditions as shown in Fig. 2. a. The E_x component of the electric field is recorded in probes positioned at the middle of the xy plane at different distances of 10, 100, 300, 600, 1200 and 1700 nm in front and behind the metamaterial. The simulation records the time signals till 6×10^{-16} s with a time step $\Delta t = 7.88 \times 10^{-17}$ s. The first part of the signals is plotted in Fig. 3. The S-parameter calculation involves the Fourier transform of the time domain signal. Therefore, a long enough simulation is required to obtain accurate results. This can be set in the *Transient Solver Parameters* window, specifying 60 dB for the *Accuracy* and choosing a *Maximum number of pulses* of 2000 in the *Specials/Steady State* entry. All results of this paper are generated with these settings.

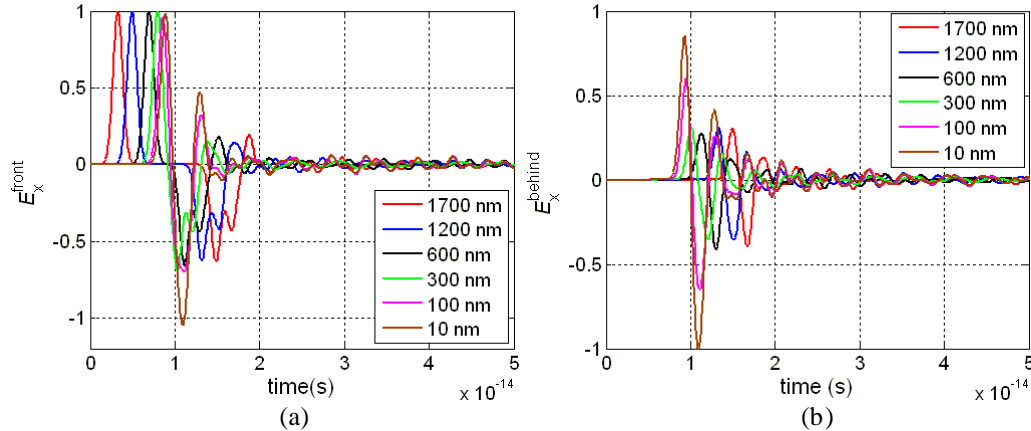


Fig. 3. The first part of the recorded electric field intensities in observation points in front and behind the fishnet structure

In time domain solutions it is difficult to control modes excited in the structure (Zsolt, this could be discussed in more detail. You can indeed excite a single mode to propagate towards the fishnet window, but you cannot suppress the higher order modes at the window because the time domain solver solves the field as a single physical object. Modes are mathematical basis functions used to express the total field in terms of eigensolutions of the infinite waveguide.) When the observation points are placed in the near field of the periodic metamaterial structure, the unwanted higher order modes (they are not really unwanted because they are needed to produce the desired response of the structure. However, for S-parameter

extraction you need to extract a single mode, which would require a processing of the field in the reference plane.) can be captured, which leads to wrong effective material parameter values. In order to obtain accurate S-parameters the observation points should be positioned far enough from the surface of the metamaterial, to sample only the dominant mode (indeed, this is the alternative way to separate the dominant propagating mode from the near field consisting of the evanescent higher order modes). Consequently, the phase delay caused by the additional distance must be compensated to determine the correct phase at the boundaries of the metamaterial.

The procedure to calculate S_{11} and S_{21} from a time domain signal is presented for the time signals recorded in the probe positioned at a distance 1700 nm from the surface of the metamaterial slab. First the reflected field E_x^{refl} is calculated by extracting from the total electric field recorded in front of the structure the incident field E_x^{inc} (see Fig. 4. a). The incident field is obtained in a second run by excluding the elements of the metamaterial from the geometry. This can be achieved by deselecting the *Consider for Simulation* checkbox in the *Local Mesh Property* window. In this way the meshing is avoided and the time signals of the two runs will have the same time step. Then the incident and the reflected signals are Fourier transformed. The magnitude and the phase of the incident and reflected complex electric fields are shown in Fig 4. b and Fig 4. c. To obtain the phases $p_{E_x^{inc}}$ and $p_{E_x^{refl}}$ at the surface of the metamaterial, as required by the effective metamaterial parameter extraction algorithm, the phase of the incident and reflected fields are corrected by assuming that they are plane waves propagating in different directions

$$p_{E_x^{inc}} = p'_{E_x^{inc}} - \varphi, \dots p_{E_x^{refl}} = p'_{E_x^{refl}} + \varphi, \quad (11)$$

where $p'_{E_x^{inc}}$ is the phase of the incident and $p'_{E_x^{refl}}$ the phase of the reflected electric field at the position of the probe, while φ is the phase delay calculated as

$$\varphi = kd = \frac{2\pi f d}{c_0} = \frac{2\pi d}{\lambda}, \quad (12)$$

where k is the wave number, d the distance between the observation point and the surface of the metamaterial, f and λ are the frequency and the wavelength of the incident electromagnetic wave. The corrected phases are plotted in Fig. 4. d. Finally, the magnitude and the phase of S_{11} can be calculated as

$$|S_{11}| = \frac{|E_x^{refl}|}{|E_x^{inc}|}, \quad p_{S_{11}} = p_{E_x^{refl}} - p_{E_x^{inc}}. \quad (13)$$

To calculate S_{21} , the transmitted time domain electric field recorded in a probe behind the structure is Fourier transformed. The phase of the transmitted electric field is corrected as

$$p_{E_x^{tr}} = p'_{E_x^{tr}} + \varphi, \quad (14)$$

where $p'_{E_x^{tr}}$ is the phase at the position of the probe and $p_{E_x^{tr}}$ the phase of the transmitted electric field at the back surface of the metamaterial. The magnitude and phase of S_{21} are obtained by normalizing the frequency domain transmitted electric field at the back surface of the metamaterial to the incident electric field at the front surface of the metamaterial

$$|S_{21}| = \frac{|E_x^{tr}|}{|E_x^{inc}|}, \quad p_{S_{21}} = p_{E_x^{tr}} - p_{E_x^{inc}}. \quad (15)$$

Please note that S_{11} corresponds to the reflection coefficient of the slab. However, S_{21} differs from the transmission coefficient by a phase angle proportional to the effective thickness of the metamaterial slab. (Zsolt, you must not correct S21 for the phase shift corresponding to the thickness of the slab. That phase shift is an intrinsic contribution of the material you want to characterize, because it has a physical thickness, otherwise you reduce the metamaterial slab to an object of zero thickness producing a phase shift corresponding to the argument of S21). The calculated S-parameters are presented in Fig. 5.

The extracted effective metamaterial parameters are presented in Fig. 6. The effective wave impedance is plotted in Fig. 6.a. Fig. 6.b shows the refractive index. In all the figures showing the refractive index, the blue line represents the imaginary part. The Kramers-Kronig approximation of the refractive

index is plotted as a black line. Possible branches of the refractive index n for $m = [-2, -1, 0, 1, 2]$ are presented as well. The real part of the refractive index n is plotted as a red line. This metamaterial slab is thin as compared to the wavelengths at which the refractive index is negative. The phase of S_{21} is continuous in the $[-180^\circ, 180^\circ]$ interval (see Fig. 5.b); consequently no branching problem occurs. The real part of the refractive index calculated with the Kramers-Kronig relation follows the branch corresponding to $m=0$. Fig. 6.c presents the extracted effective electric permittivity and magnetic permeability. The figure of merit $FOM = -n/\kappa$ characterizes the performance of metamaterials. In this case the maximum value of FOM is around 3, see Fig. 6.d.

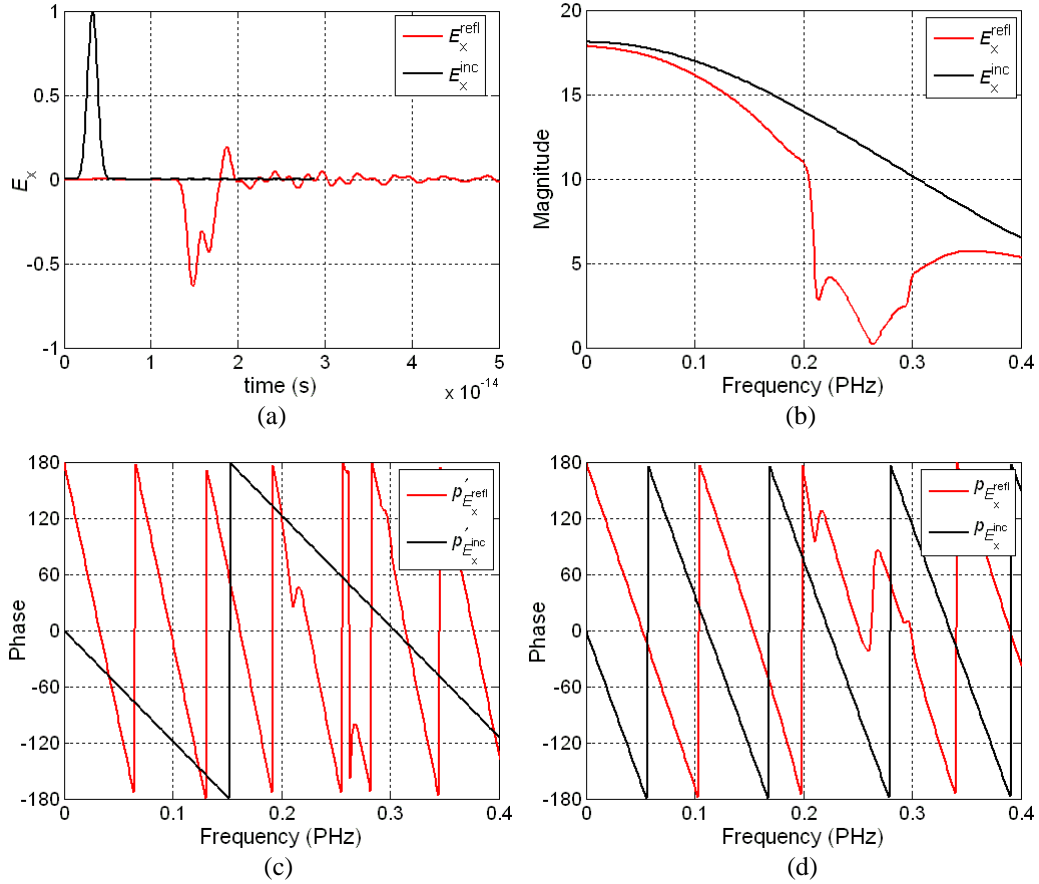


Fig. 4. Procedure to calculate S_{11} from time domain signal. In (a) the early part of the recorded incident and reflected electric field is presented, (b) shows the magnitudes and (c) the phases at the location of the probes while (d) plots the corrected phases at the surfaces of the metamaterial.

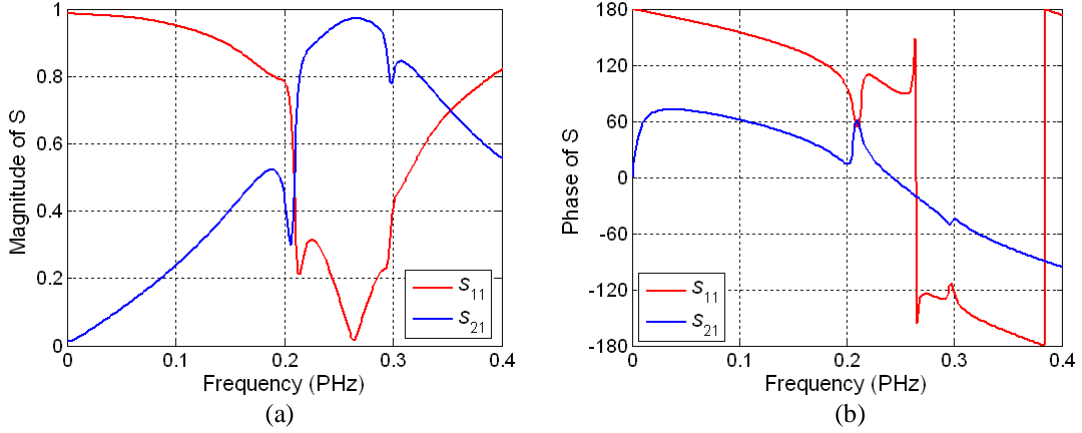


Fig. 5. The magnitude and phase of the S-parameters calculated from the time domain signal of probes located in front and behind the fishnet structure at a distance of 1700 nm.

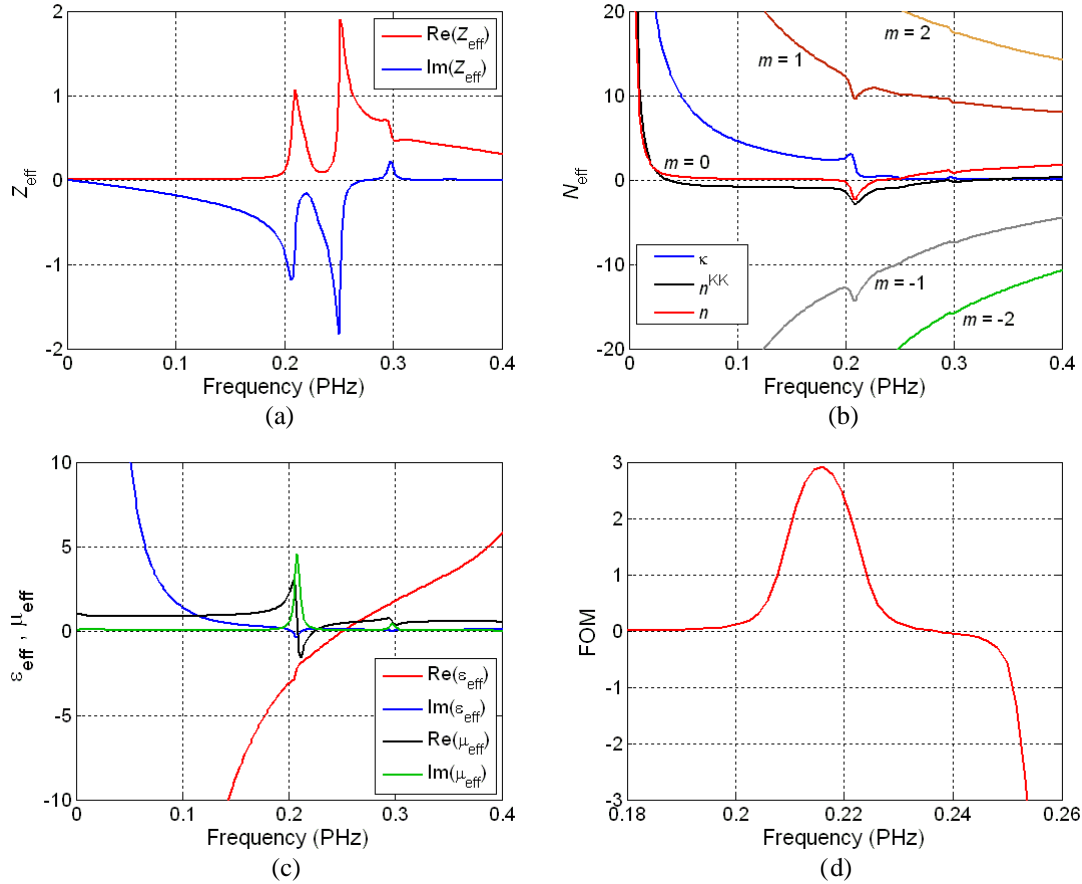


Fig. 6. Extracted effective metamaterial parameters for the fishnet structure. (a) presents the wave impedance, (b) the real and imaginary part of the refractive index, the Kramers Kronig approximation and several branches, (c) the electric permittivity and magnetic permeability and (d) the figure of merit.

The phase of S_{21} yields useful information on several facts. If the phase change exceeds 180° , then more than one branch of the logarithmic function can contribute to the refractive index. In addition it can also indicate the frequency range in which the refractive index can be negative. Comparison of Fig. 5.b and Fig. 6.c, reveals that whenever the refractive index becomes negative, the slope of the phase S_{21} changes sign. However, a sign change in the slope of S_{21} not necessarily implies negative refractive index,

but it may indicate such an occurrence. This can be explained by the opposite orientations of the group and the phase velocity in the double negative region [4].

Fig. 7 compares the S-parameters calculated from the time signals of the probes positioned at different distances from the surface of the metamaterial slab. As the figures show, the S-parameters calculated at the observation points positioned at 600 nm and 1700 nm are very similar. However the probes positioned at 10 nm, 100 nm and 300 nm produce wrong S-parameters, because the near-field of the fishnet structure extends more than 300 nm from its surface. This fact demonstrates a long range electromagnetic coupling between the metamaterial unit cells.

In case of new metamaterial designs it is strongly recommended to study the convergence of the S-parameter magnitudes by comparing the results extracted at different probe positions and to visualize the electromagnetic fields around the structure.

This modeling setup with periodic boundary conditions (Zsolt, are these Floquet boundary conditions or PEB and PMB conditions?) and plane-wave excitation has the advantage that it provides the complete time evolution of the electromagnetic fields in the computational volume. In addition it allows the user to have full control over the calculation of the S-parameters. In case of specular reflection, the regime in which the structures behaves as metamaterial, the time signal of the electric field in one observation point in front and one behind the metamaterial slab is sufficient to extract the effective metamaterial parameters.

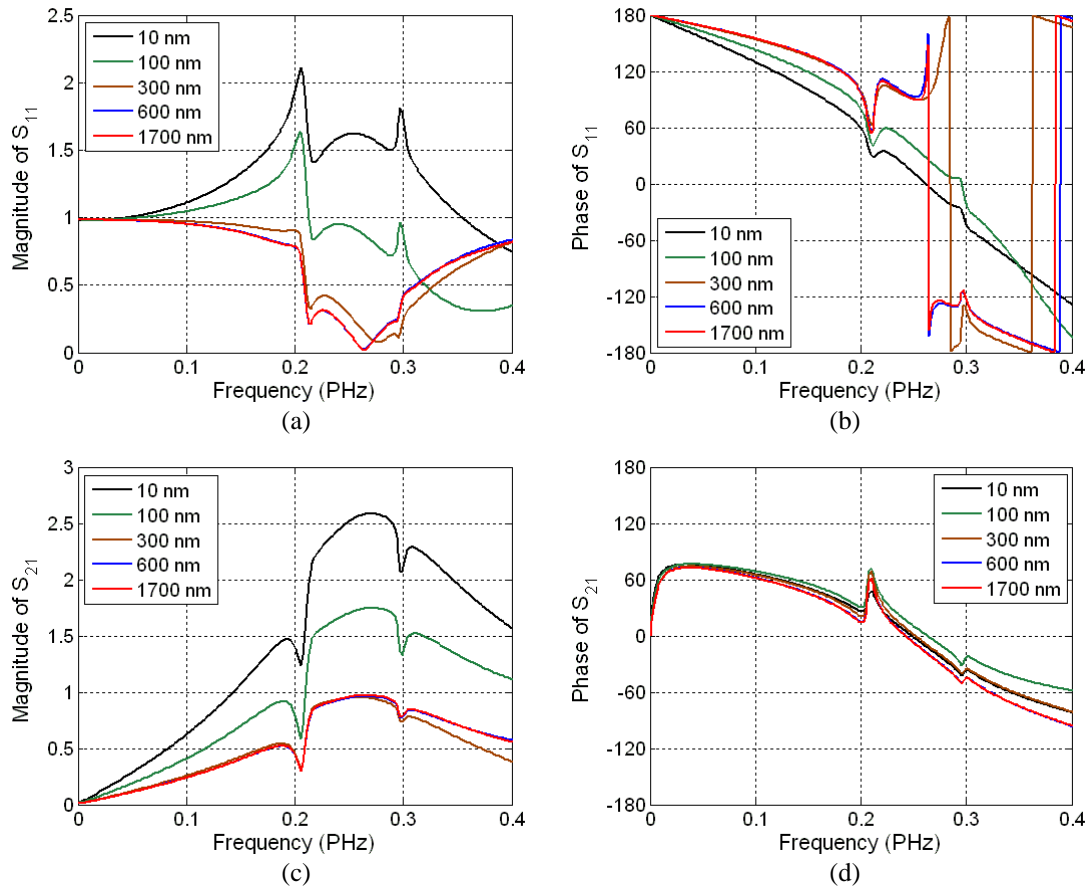


Fig. 7. Comparison of the S-parameters calculated in observation points positioned at different distances from the surface of the metamaterial slab.

3.2 S-parameter calculation with time domain solver specifying PEC-PMC boundary conditions and waveguide ports for excitation

Consider a plane wave propagating in free space in z direction with the components E_x and H_y . This is equivalent to the propagation of the fundamental mode in a rectangular parallel-plate waveguide. In CST Microwave Studio this can be realized by considering a rectangular computational space and setting the tangential component of the electric field to zero (PEC boundary condition) on the boundaries in x direction and the tangential component of the magnetic field to zero (PMC boundary condition) on the boundaries in y direction.

This setup can be applied to calculate the S-parameters of metamaterials as shown in Fig. 2.b. In addition, due to the symmetry of the fishnet structure, the computational volume can be reduced to one quarter by specifying symmetry planes. This can be set up in the *Boundary Conditions/Symmetry planes*, by specifying zero tangential electric field in the *YZ plane* combo box and zero tangential magnetic fields in the *XZ plane* combo box. S-parameters are automatically calculated when the model is excited by waveguide ports.

To obtain accurate results, the port is positioned at a sufficiently large distance from the surface of the metamaterial. The phase shift can be easily corrected by ‘deembedding’ the port. By adjusting, in the *Ports/Properties/Distance to reference plane* edit box, the negative of the distance between the port and the surface of the metamaterial, the solver produces the required phases of the S-parameters. In this way the full effective metamaterial parameter extraction procedure is simplified to a great extent.

3.3 S-parameter calculation with frequency domain solver, unit cell boundary conditions and Floquet ports excitation

The S-parameters can be calculated with the frequency domain solver as well, for example by specifying unit cell boundary conditions and Floquet ports for excitation. In case of frequency domain solvers the user has full control over the modes which are excited, consequently the ports can be positioned in the close neighborhood of the metamaterials (Zsolt, are you sure of this? Normally, whether you solve in the time domain or in the frequency domain at one frequency, the ports must either be sufficiently away, or the field in the ports must be processed to extract the fundamental mode content by convolution). Usually the first or second Floquet mode is excited (they are perpendicular to each other). The required phases can be obtained by ‘deembedding’ the port.

To compare the accuracy of the presented calculation schemata, the difference between the magnitudes of S-parameters is presented in Fig. 8. In case of the time domain solver and periodic boundary conditions (TD PBC) the probe is positioned at 1700 nm. The ports are 600 nm away from the metamaterial when the PEC/PMC boundary conditions are applied. When the frequency domain solver and unit cell boundaries are used, the Floquet port is positioned 10 nm away from the surface of the metamaterial. As Fig. 8 shows, the simulations give very similar results.

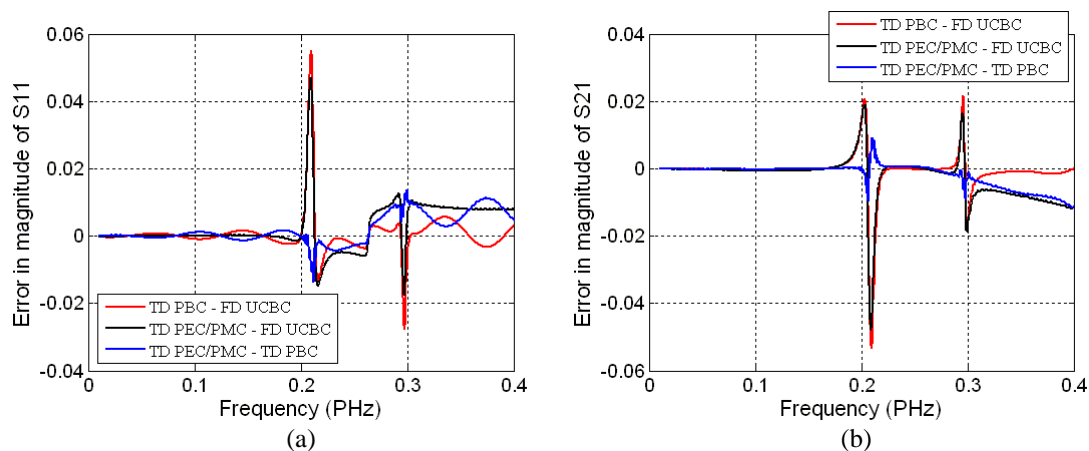


Fig 8. The difference of the S-parameters, calculated in three different ways, for the fishnet structure.

4. Field monitors to understand the origin of the negative refractive index

To understand the behavior of the fishnet structure and the origin of the negative refractive index, the electromagnetic field distributions at resonances can be conveniently investigated by the *Field Monitors* provided by CST. To determine the exact location of the resonances, from the calculated S-parameters the absorbance A can be determined as

$$A = 1 - T - R = 1 - |S_{21}|^2 - |S_{11}|^2, \quad (16)$$

where T denotes the transmittance and R the reflectance of the metamaterial slab. Fig. 9 shows the calculated absorbance of the fishnet structure. As it can be observed, in the frequency range of interest there are two resonant peaks at frequencies 0.2074 PHz and 0.2953 PHz.

Comparing the absorbance with the extracted effective material parameters plotted in Fig. 6 it can be seen that the location of the first resonant peak is in the frequency region of the negative refractive index. However the exact location of the absorbance peak does not correspond neither to the position of the peak in the imaginary part of the electric permittivity neither to the peak in the imaginary part of the magnetic permeability. Under some circumstances [24] the metamaterials can be represented as a collection of electric and magnetic dipoles. However, in case of metamaterials these dipoles are not independent of each other [15].

After the identification of the resonant frequencies, a second simulation can be performed to reveal the distribution of the electric and magnetic fields and of the current density in the fishnet structure. To reduce the amount of data the field distributions can be saved in two dimensional cross sections of the computational domain. In the *Solve/Field Monitors* the radio buttons offers the possibility to select the type of the field monitors. By specifying the values of the resonant frequencies in the *Frequency* entry, the monitor will record the chosen field type only for that particular frequency.

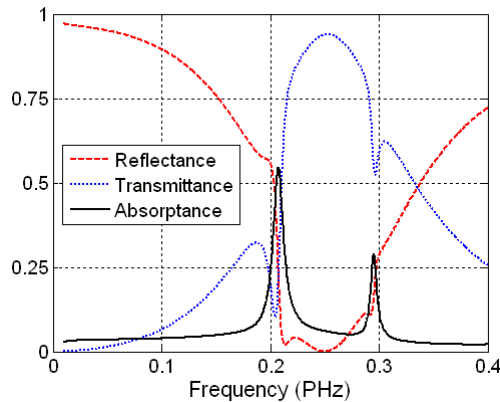


Fig. 9. The reflectance, transmittance and absorbance of the fishnet structure

Fig. 10 presents the current density distributions of the upper part at the first absorbance resonance. The animation of the fields reveals that the current density is concentrated in the metallic parts. In a similar way as it was presented in [30], the simulations shows that the antiparallel current flow generated by the coupling of the H_y component of the field to the loop formed by the horizontal sections of the fishnet is responsible for the resonant magnetic behavior. The currents in the vertical sections are also antiparallel to each other and they flow in opposite direction to those in horizontal areas.

The distribution of the magnetic field intensity in the $y\bar{z}$ plane is presented in Fig. 11. The figure shows clearly that the near field extends a large distance compared to the thickness of the structure in agreement with the results presented in Fig 7. By replacing the fishnet structure with a homogeneous slab the far field behavior can be predicted, however there is no possibility to describe the near field behavior. As it is presented in the next section, long range coupling occurs when more layers are considered in the fishnet structure. This leads to the fact that the extracted effective material parameters are not independent of the thickness of the structure; consequently their meaning should be reconsidered.

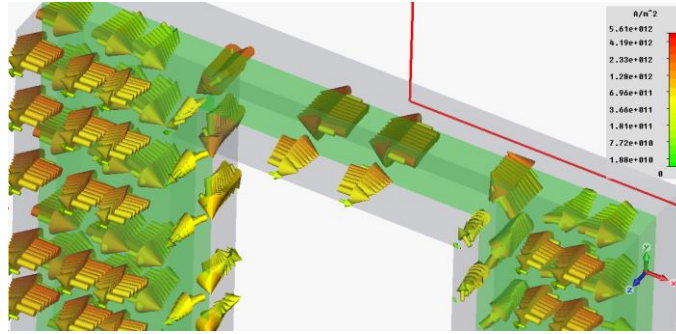


Fig. 10. The distribution of the current density in the upper part of the fishnet structure

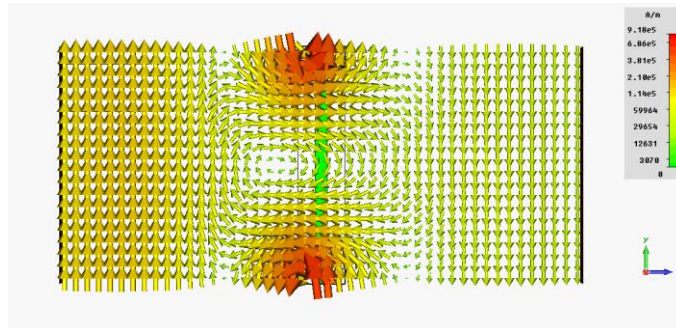
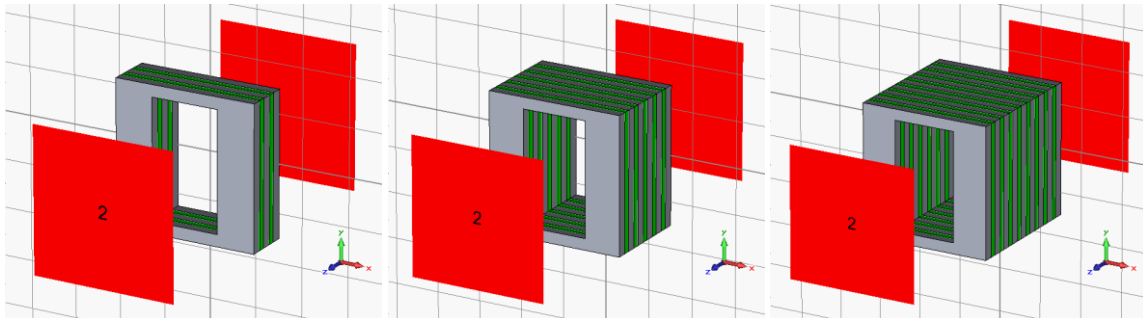


Fig. 11. The distribution of the magnetic field intensity in the yz plane

The animations obtained from the CST simulations provides a visual picture of the time and space evolution of the electromagnetic energy and field leading to a better understanding of the complex physical phenomena which take place in metamaterial structures. Such animations may be also helpful in university courses on photonics.

5. Multilayer fishnet structure

In this section the effective metamaterial parameters of multilayer fishnet structures are calculated and compared. As it was show in [1], [29], [30] for the frequencies where the refractive index of the metamaterial is -1 and the losses are negligible, the perfect image of an object can be formed. However the position of the object cannot be arbitrary. It should be positioned at a distance which is half of the effective thickness of the metamaterial. Because it is difficult to control small distances, it is more convenient to fabricate metamaterial with larger thickness. The multilayer fishnet is one of the promising approaches. The investigated structures are composed of three, six and nine silver layers separated by MgF_2 layers as shown in Fig. 12. The corresponding effective metamaterial thicknesses are 195 nm, 420 nm and 645 nm. As the number of layers is increased, the thickness of the metamaterial becomes comparable to the wavelength, and the effective medium theory cannot be applied anymore to extract meaningful metamaterial parameters and to represent the electromagnetic behavior of the structures. This will be explained below.

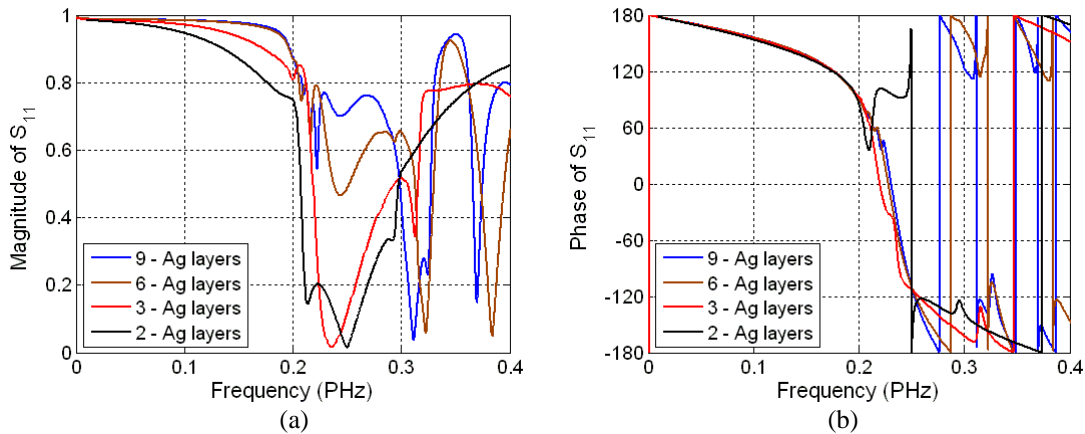


(a) (b) (c)
 Fig. 12. Multilayer fishnet structures with (a) three layers of silver separated by two layers of MgF₂ (b) six layers of silver separated by five layers of MgF₂ and (c) nine layers of silver separated by eight layers of MgF₂

The electromagnetic field computations were performed with the time domain solver, specifying PEC/PMC boundary conditions and waveguide ports for excitation positioned 600 nm from the surface of the metamaterials. In this section the metamaterial is embedded in an effective dielectric medium with $\epsilon_r = 1.21$ as in [15]. The aim of the calculation is to determine the effective parameters of these metamaterials in the frequency range from 0.1 to 0.4 PHz. Simulations show that this metamaterial presents many resonances outside of this frequency range. Therefore, to get a good estimate for the Kramers-Kronig integral, the simulations cover the 0 to 1 PHz frequency interval. We found that by increasing this frequency interval even further the accuracy of the Kramers-Kronig approximation does not change noticeably.

In Fig. 13 the variation of the S-parameters in function of the number of fishnet layers is presented. It appears that the number of layers affects the S-parameters to a great extent. This fact indicates again the long range electromagnetic coupling between the metamaterial unit cells.

It should be mentioned that meaningful material parameters are independent of the material thickness, or that at least they should converge as the material thickness is increased. The extracted effective wave impedance and refractive index are presented in Fig. 14. As it is expected by comparing the S-parameters, the extracted effective metamaterial parameters differ considerable from each other. Fig. 14. c presents the real part of the refractive index as a function of the number of layers in the resonant frequency region. By investigating the continuity of the real part of the refractive index it appears that a first discontinuity occurs at $f = 0.2161$ PHz in case of 6 layers and at $f = 0.2096$ PHz in case of 9 layers. Fig. 15 reveals the details of the calculation; by inspecting possible branches the origin of the discontinuity can be understood. In both cases, at low frequencies the refractive index follows the zero branches. As it can be observed at higher frequencies the Kramers-Kronig approximation again follows the zero branch very accurately. However there is no branch in the resonant frequency region which can connect the two regions in a continuous way. At resonance, the thickness of the samples becomes comparable to the optical wavelength, and the effective medium theory cannot be applied anymore. If one decides to select the branch based solely on continuity of the refractive index, then starting from the first discontinuity point, a branch with higher and higher branch number should be followed, and as the frequency is increased, the refractive index will diverge. Therefore, we interpret the first discontinuity as an upper limit of the effective medium theory.



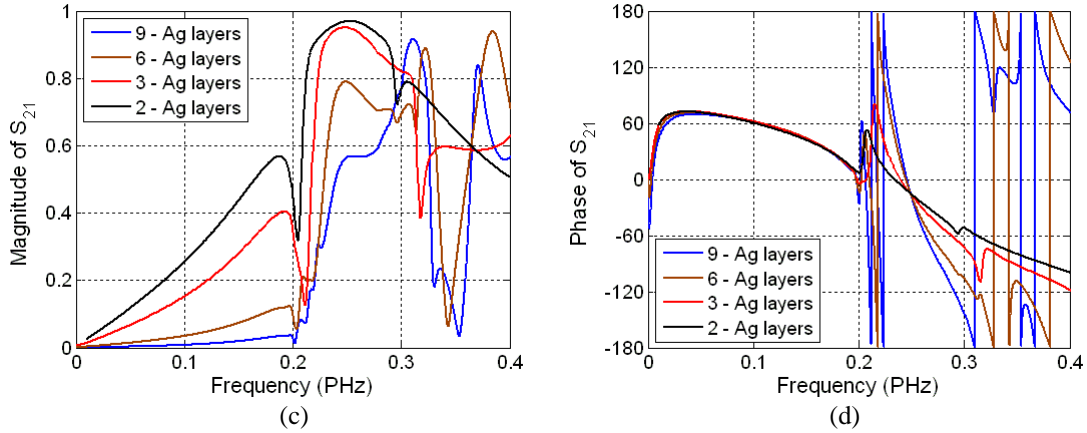


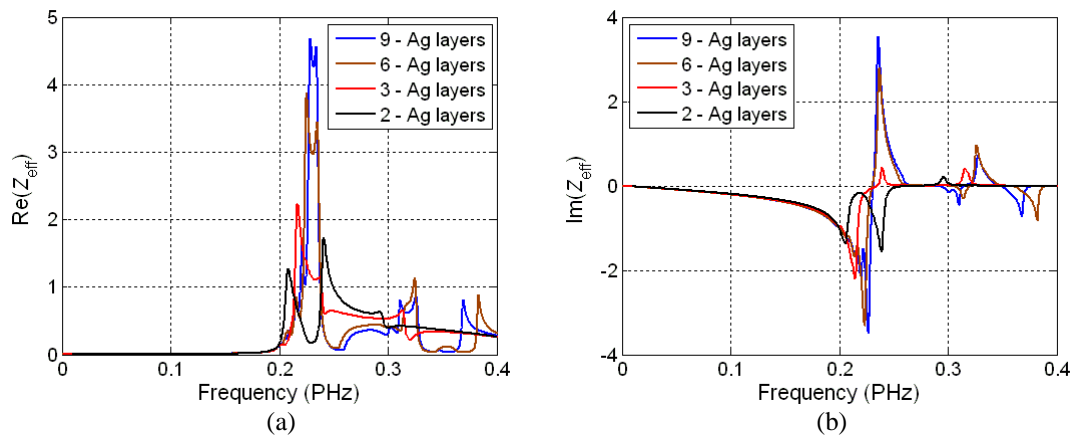
Fig. 13. Variation of the S-parameters with increasing number of fishnet layers.

When many layers of unit cells are present, the electromagnetic material properties should converge to a bulk value. However, by comparing the retrieved effective metamaterial parameters for different thicknesses we observe that the effective medium theory breaks down before convergence occurs. This is due to the fact that the geometrical feature sizes are of the order of the wavelength in the frequency range of interest.

Conclusions

We have presented a calculation methodology based on S-parameters, Fresnel-Airy formulas and Kramers-Kronig relations to extract the effective parameters of metamaterial. The details of the S-parameter calculations with CST Microwave Studio were presented. The flexibility of the software permits to perform the calculations in many different ways. However, the time domain solver fits better to the extraction algorithm, because large frequency ranges can be covered in a single run, and the truncation error in the Kramers Kronig integral can thus be reduced. At the same time, special attention must be paid to the positioning of the observation points to exclude the effect of the higher order modes.

The results obtained with the Kramers-Kronig relations give a suitable approximation for the real part of the refractive index. When the metamaterial is thick compared to the wavelength, more than one branch can be involved in the final result. As the optical thickness becomes comparable to the wavelength, the effective medium theory cannot be applied anymore. The discontinuity of the refractive index indicates that the limit of the effective medium theory has been reached.



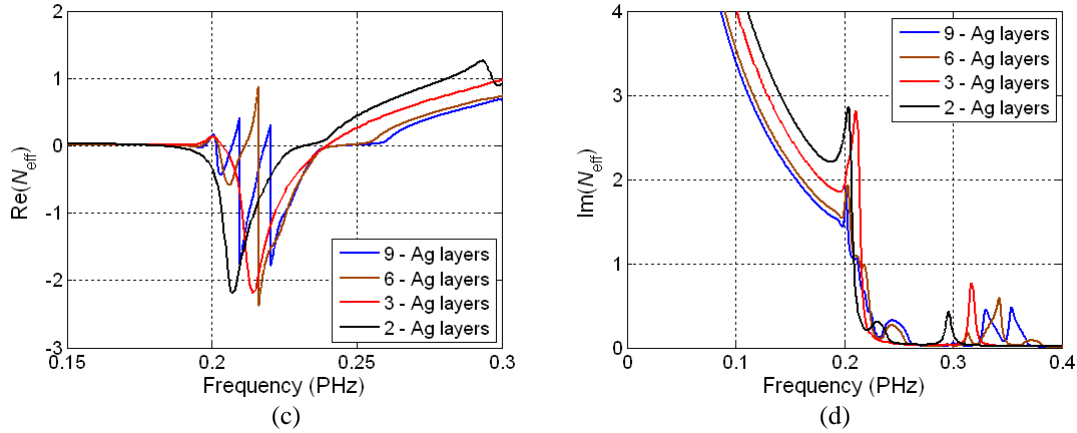


Fig. 14. Variation of the extracted effective parameters in function of the number of layers.

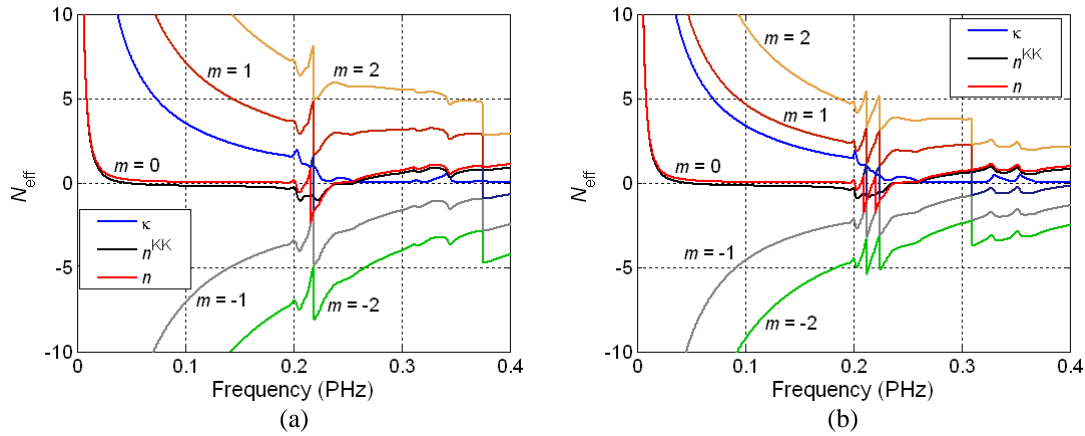


Fig. 15. The real and imaginary part of the refractive index, the Kramers Kronig approximation and several branches for the 6 and 9 layer thick metamaterial.

References

- [1] V. G. Veselago, The electrodynamics of substances with simultaneously negative values of ϵ and μ , *Sov. Phys. Usp.*, 10, 4, 1967, pp.509–514.
- [2] D. R. Smith, W.J. Padilla, D.C. Vier, S.C. Nemat-Nasser, S. Schultz, Composite Medium with Simultaneously Negative Permeability and Permittivity, *Phys. Rev. Lett.*, 84, 2000, 4184.
- [3] I. Tsukerman, *Computational Methods for Nanoscale Applications*. Springer, 2008, pp. 446–477.
- [4] R. Marqués, F. Martín, and M. Sorolla, *Metamaterials with Negative Parameters*. John Wiley and Sons, 2008.
- [5] D. J. Griffiths, *Introduction to Electrodynamics*. Benjamin Cummings, 3 edition, 1999, pp. 327–328.
- [6] P. A. M. Dirac, Quantised Singularities in the Electromagnetic Field, *Proc. Roy. Soc.*, 133, 60, 1931.
- [7] J. B. Pendry, A. J. Holden, W. J. Stewart, I. Youngs, Extremely Low Frequency Plasmons in Metallic Microstructures, *Phys. Rev. Lett.*, 76, 1996, pp. 4773–4776.
- [8] J. B. Pendry, A. J. Holden, D. J. Robbins. W. J. Stewart, Magnetism from Conductors, and Enhanced Non-Linear Phenomena, *IEEE Trans. Microwave Theory Tech*, 47, 2075, 1999.
- [9] D. R. Smith, W. J. Padilla, D. C. Vier, S. C. Nemat-Nasser, S. Schultz, Composite medium with simultaneously negative permeability and permittivity, *Phys. Rev. Lett.*, 84, 18, May 2000, pp. 4184–4187.
- [10] R. A. Shelby, D. R. Smith, S. Schultz, Experimental verification of a negative index of refraction, *Science*, 292, 5514, 2001, pp. 77–79.
- [11] V. M. Shalaev, Optical negative-index metamaterials. *Nature Photonics*, 1, 2006, pp. 41–48.
- [12] S. Zhang, W. Fan, K.J. Malloy, S.R. Brueck, N.C. Panoiu, R.M. Osgood, Near-infrared double negative metamaterials, *Opt. Express*, 13, 13, 2005, pp. 4922–4930.

- [13] S. Zhang, W. Fan, K. J. Malloy, S. R.J. Brueck, N. C. Panoiu, R. M. Osgood, Demonstration of metaldielectric negative-index metamaterials with improved performance at optical frequencies. *J. Opt. Soc. Am. B*, 23, 3, 2006, pp. 434–438.
- [14] G. Dolling, M. Wegener, C. M. Soukoulis, S. Linden, Negative-index metamaterial at 780 nm wavelength, *Opt. Lett.*, 32, 1, 2007.
- [15] G. Dolling, C. Enkrich, M. Wegener, C. M. Soukoulis, S. Linden, Low-loss negative index metamaterial at telecommunication wavelength, *Opt. Lett.*, 31, 2006, pp. 1800–1802.
- [16] A. Alù, F. Bilotti, N. Engheta, L. Vegni, Theory and Simulations of a Conformal Omni-Directional Subwavelength Metamaterial Leaky-Wave Antenna, *IEEE Trans. Ant. Prop.*, 55, 6, 2007, pp. 1698- 1708.
- [17] A. Alù, M. G. Silveirinha, A. Salandrino, N. Engheta, Epsilon-Near-Zero (ENZ) Metamaterials and Electromagnetic Sources: Tailoring the Radiation Phase Pattern, *Phys. Rev B*, 75, 155410, 2007.
- [18] C. Garcia-Meca, R. Ortuno, F.J. Rodríguez-Fortuno, J. Martí, A. Martínez, Strong magnetism at visible wavelengths via coupled silver nanohoops, Proc. of the 3rd Int. Congress on Advanced Electromagnetic Materials in Microwaves and Optics, London, 2009, pp. 767-769.
- [19] X. Chen, T. M. Grzegorzczak, B. I. Wu, J. Pacheco, J. A. Kong, Robust method to retrieve the constitutive effective parameters of metamaterials, *Phys. Rev. E*, 70, 016608, 2004.
- [20] D. R. Smith, D. C. Vier, T. Koschny, C. M. Soukoulis, Electromagnetic parameter retrieval from inhomogeneous metamaterials, *Phys. Rev. E*, 71, 036617, 2005.
- [21] V. Varadan, R. Ro, Unique retrieval of complex permittivity and permeability of dispersive materials from reflection and transmitted fields by enforcing causality, *IEEE Trans. Microwave Theory Tech.*, 55, 10, 2007, pp. 2224–2230.
- [22] G. Lubkowski, R. Schumann, T. Weiland, Extraction of effective material parameters by parameter fitting of dispersive models, *Microw. Opt. Techn. Lett.*, 49, 2, 2007, pp. 285–288.
- [23] D. R. Schmidt, J. B. Pendry, Homogenization of metamaterials by field averaging, *J. Opt. Soc. Am. B.*, 23, 3, 2006, pp. 391-403.
- [24] C. R. Simovski, Analytical modelling of double-negative composites, *Metamaterials*, 2, 4, 2008, pp. 169-185.
- [25] Zs. Szabó, G. Park, R. Hedge, E. Li, Electromagnetic parameter extraction technique of metamaterials applying the Kramers-Kronig relations, submitted to *IEEE Trans. Microwave Theory Tech.*, 2009.
- [26] P. K. Chattopadhyay, *Mathematical Physics*. John Wiley and Sons, 1990, pp. 23–24.
- [27] E. Palik, Ed., *Handbook of Optical Constants of Solids I-IV*. Academic Press, 1985-1998.
- [28] M. Kafesaki, I. Tsiapa, N. Katsarakis, Th. Koschny, C. M. Soukoulis, E. N. Economus, Left-handed metamaterials: The fishnet structure and its variations, *Phys. Rev. B*, 75, 235114, 2007.
- [29] J. B. Pendry, Negative Refraction Makes a Perfect Lens, *Phys. Rev. Lett.*, 85, 3966, 2000.
- [30] D. R. Smith, D. Schurig, M. Rosenbluth, S. Schultz, S. Anantha Ramakrishna, J. B. Pendry, Limitations on subdiffraction imaging with a negative refractive index slab, *Appl. Phys. Lett.*, 82, 10, 2003, pp.1506-1508.